Suppressing spatio-temporal lasing instabilities with wave-chaotic microcavities

Stefan Bittner,[1] Stefano Guazzotti,[2] Yongquan Zeng,[3]
Xiaonan Hu,[3] Hasan Yılmaz,[1] Kyungduk Kim,[1] Sang Soon Oh,[2,4]
Qi Jie Wang,[3] Ortwin Hess,[2*] Hui Cao[1*]

[1]Department of Applied Physics, Yale University, New Haven,
Connecticut 06520, USA

[2]Blackett Laboratory, Department of Physics, Imperial College London,
London SW7 2AZ, United Kingdom

[3]Center for OptoElectronics and Biophotonics, School of Electrical and
Electronic Engineering and The Photonics Institute, Nanyang Technological University,
50 Nanyang Avenue, 639798 Singapore

[4]School of Physics and Astronomy, Cardiff University,
Cardiff CF24 3AA, United Kingdom

[*]To whom correspondence should be addressed;
E-mail: hui.cao@yale.edu, o.hess@imperial.ac.uk

Spatio-temporal instabilities are widespread phenomena resulting from complexity and nonlinearity. In broad-area edge-emitting semiconductor lasers, the nonlinear interactions of multiple spatial modes with the active medium can result in filamentation and spatio-temporal chaos. These instabilities degrade the laser performance and are extremely challenging to control. We demonstrate a powerful approach to suppress spatio-temporal instabilities using wave-chaotic or disordered cavities. The interference of many propagating waves with random phases in such cavities disrupts the formation of self-

organized structures like filaments, resulting in stable lasing dynamics. Our method provides a general and robust scheme to prevent the formation and growth of nonlinear instabilities for a large variety of high-power lasers.

Systems with complex spatio-temporal dynamics can exhibit instabilities and even chaotic dynamics, as seen for example in weather patterns, turbulent flow, population dynamics (*1*), or chemical reactions (*2*). Beyond natural occurrences, spatio-temporal instabilities also appear in sophisticated technological systems such as fusion reactors exhibiting plasma instabilities (*3*) or type-II superconductors with complex vortex dynamics (*4*). Lasers are another important class of systems exhibiting inherent spatio-temporal instabilities and deterministic chaos due to the nonlinear interaction of the light field with the active medium (*5–7*). The underlying nonlinearities are particularly pronounced for high power lasers, which have a large transverse area and operate on many spatial (transverse) modes. Nonlinear modal interactions entail spatio-temporal instabilities such as irregular pulsation and filamentation, e.g., in broad-area edge-emitting semiconductor lasers (*8–14*), that degrade the spatial, spectral and temporal properties of the emission.

Because of wide-spread applications of high power lasers in material processing, large-scale displays, laser surgery and pumping sources, much effort has been invested in suppressing lasing instabilities. Most strategies proposed seek to reduce the level of complexity by reducing the number of lasing modes. For broad-area semiconductor lasers, this can be achieved by external control, e.g., through injection of a coherent signal (*15, 16*) or delayed optical feedback (*17–19*), or schemes based on Parity-Time symmetry (*20, 21*). Successful with moderate powers, these approaches quickly become less effective when increasing the cavity size in order to harness more power. An external control signal applied via injection or feedback through the cavity boundary has a diminished effect deep inside a large cavity and it thus fails to control the dynamics over the whole cavity. Furthermore, these approaches are typically sensitive to

external perturbations and require a careful adjustment of parameters to reach stabilization.

Our approach aims to eliminate spatio-temporal instabilities in broad-area edge-emitting semiconductor lasers without reducing the number of lasing modes and is thus applicable to high power operation. Instead of suppressing the filaments via external signals, we disrupt the coherent nonlinear processes that lead to their formation by using cavities with complex spatial structure to create many propagating waves with random phases. The complex interference of these waves prevents the formation of self-organized structures such as filaments that are prone to modulational instabilities. We demonstrate the generality and robustness of this approach through experiments and numerical simulations with two different systems, (i) two-dimensional (2D) microcavities featuring chaotic ray dynamics and (ii) one-dimensional (1D) cavities with random fluctuations of the refractive index. The chaotic ray dynamics and the structural disorder are responsible for the creation of multi-wave interference effects, respectively.

Conventional broad-area edge-emitting lasers

We first show the complex spatio-temporal dynamics of GaAs quantum well (QW) lasers in the widely-used stripe geometry. The reflections from two cleaved facets in the longitudinal direction (parallel to the stripe axis) and gain guiding in the transverse direction (perpendicular to the stripe axis) provide optical confinement [see methods (*22*)]. Spatio-temporal traces of the lasing emission intensity at one end facet were measured by a streak camera with picosecond resolution [see methods (*22*)]. As shown in Figure 1A, the lasing emission is spatially concentrated at multiple locations — so-called filaments — which sometimes move in the transverse direction (*8–10*). Emission patterns measured during the same pulse in Fig. S5 demonstrate that the lasing emission can change suddenly from a nearly uniform distribution to concentration in small regions or filaments. Such diverse emission profiles illustrate that the formation of filaments is an inherent feature of the lasing dynamics and not due to inhomogeneities of the ca-

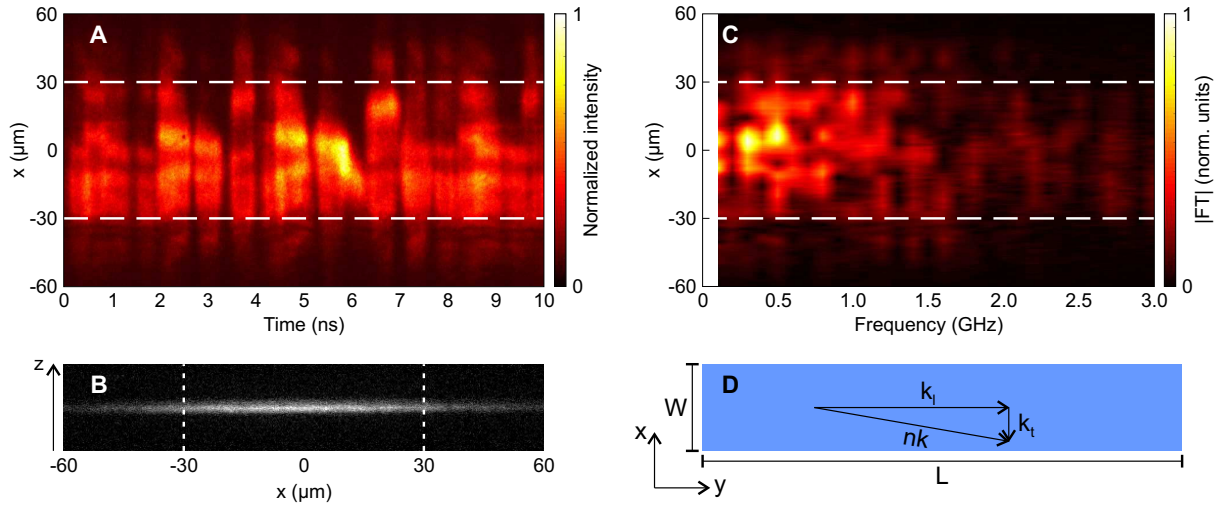

Figure 1: Spatio-temporal instabilities of an electrically pumped edge-emitting semiconductor laser. The top metal contact is 60 μm wide and 0.98 mm long. (**A**) Spatio-temporal image of the emission intensity $I(x,t)$ at one of the cleaved facets. The stripe laser was injected with an electric current of 400 mA and 2 μs-long pulses, where the lasing threshold current was $I_{th} = 230$ mA. The image was taken at 0.37 μs after the start of the pump pulse, well beyond any turn-on transient. Part of the emission stems from outside the region of the top contact (marked by white dashed lines) due to lateral spread of the injected current in the GaAs. (**B**) Image of electroluminescence from the end facet for 100 mA pump current (below threshold) and a pulse length of $t_p = 20$ μs. The emission is spatially homogeneous without any visible defects. (**C**) Temporal Fourier transform of $I(x,t)$ in (A). (**D**) Sketch of a rectangular Fabry-Perot cavity of length L and width W where $L \gg W$. The wave vector can be separated into longitudinal and transverse components k_l and k_t, respectively. Since $k_l \gg k_t$, the lasing modes propagate predominantly in the longitudinal (y) direction.

vity. This is confirmed by an electroluminescence image (Fig. 1B) taken below lasing threshold displaying a homogeneous intensity distribution across the facet. Furthermore, the lasing emission oscillates rapidly and irregularly in time (Fig. 1A). The spatially-resolved temporal Fourier transform of the emission intensity $I(x,t)$ (Fig. 1C) reveals a number of frequency components up to about 1.5 GHz, which accounts for the irregular oscillations on a nanosecond time scale.

The filaments are formed through spatio-temporal nonlinear processes including spatial hole burning, carrier-induced index variation and self-focusing (*8–14*). The stripe laser cavity is of

Fabry-Perot (FP) type, and the light field propagates predominantly in the longitudinal direction. The wave vector component in the longitudinal direction, k_l, is much larger than that in the transverse direction, k_t. Consequently, the transverse wavelength $\lambda_t = 2\pi/k_t$ is typically on the order of a few micrometers, and much longer than the longitudinal wavelength $\lambda_l = 2\pi/k_l$. A variation of the field intensity in the transverse direction on the scale of λ_t can result in filamentation due to carrier-induced index changes: a region of increased intensity depletes the gain, thus raising the refractive index locally and forming a lens. The lens will focus light and further enhance local intensity. This self-focusing process generates a filament with a typical width of several micrometers, comparable to the transverse wavelength. Since the optical gain is less depleted outside the filament, the filament tends to migrate transversely to the neighboring region of higher gain. Meanwhile, additional filaments may form at locations of less carrier depletion. These filaments will interact nonlinearly via the semiconductor quantum well. Due to dynamic gain and nonlinear interaction, the filaments vary in space and time, leading to complex spatio-temporal dynamics and instabilities (*9*). The resulting degradation and temporal fluctuations of the output profile limit the laser applications.

Wave-chaotic microcavity lasers

Microcavities with chaotic ray dynamics (*23–25*) have been studied in the context of wave-dynamical chaos (*26*). The resonant modes of the passive cavities are determined by a linear wave equation and do not exhibit chaos in the sense of an exponential sensitivity to the initial conditions. However, the chaotic ray dynamics manifests in the spatial and spectral properties of the cavity resonances, e.g., the spatial field distributions feature a pseudo-random, speckle-like structure. Such wave-chaotic microcavities have been used to tailor the steady-state lasing properties such as output directionality, lasing threshold and spectrum (*23–25, 27, 28*). Here we investigate the temporal dynamics of such lasers.

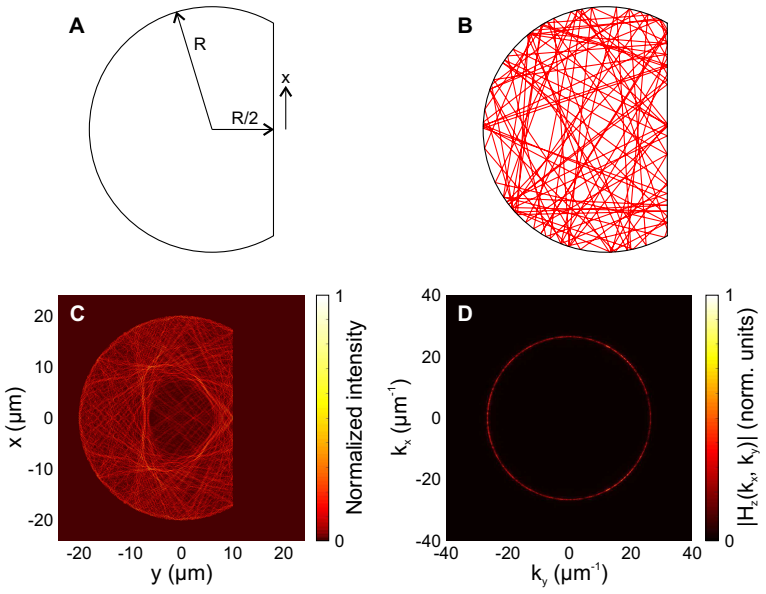

Figure 2: D-cavity with chaotic ray dynamics. (**A**) Geometry of the D-cavity. A section is removed from a circle with radius R along a straight cut $R/2$ away from the center. The coordinate along this segment of the boundary is denoted by x. (**B**) A typical ray trajectory in a closed D-cavity covers the entire cavity and propagates in all directions. (**C**) Intensity distribution of a typical high-Q mode ($\lambda = 800.4$ nm, $Q = 3443$) in a dielectric D-cavity with radius $R = 20\ \mu$m and refractive index $n = 3.37$. (**D**) The wave-vector distribution of the same mode is isotropic, indicating there is no dominant direction of propagation.

As an example, we consider a D-shaped cavity (Fig. 2A), which has fully chaotic ray dynamics. A single trajectory (Fig. 2B) generally covers the entire cavity and propagates in all possible directions. The classical ray dynamics manifests in the spatial structure of the resonant modes (Fig. 2C). The intensity distribution features an irregular, pseudo-random structure, reminiscent of a speckle pattern with an average grain size of $\lambda/(2n)$, where n is the refractive index. The characteristic length scale is isotropic, in contrast to the FP-cavity modes that feature a larger transverse than longitudinal wavelength. The wave-vector distribution (Fig. 2D) reveals that the D-cavity mode is a superposition of numerous plane waves in all possible directions.

These features of the chaotic cavity modes directly affect the lasing dynamics: since the spatial structure of the modes is so fine-grained in all directions, the spatial extent of field

intensity variations is too small to create a lensing effect, and additionally there are no dominant propagation directions that light could be focused to. These qualitative differences of the mode structure and the associated length scales compared to FP-cavities result from complex multi-wave interference and can prevent the formation of coherent spatio-temporal structures such as filaments.

We fabricated D-cavity lasers by photolithography and wet or dry (reactive ion) etching [see methods (*22*)]. Figure 3A shows a SEM image of a cavity fabricated by reactive ion etching. Figure 3B is the spatio-temporal trace of the lasing emission intensity, $I(x,t)$, at the straight segment of the boundary of the D-cavity. Compared to the emission trace in a 10 ns-long interval for the stripe laser (Fig. 1A), the D-cavity laser emission has nearly constant intensity and does not exhibit rapid pulsations. The temporal Fourier transform of $I(x,t)$ in Fig. 3C confirms the absence of GHz frequency oscillations, in contrast to Fig. 1C. The spatio-temporal trace of the D-cavity laser (Fig. 3D) over a time interval of 1.5 μs reveals temporal fluctuation of the emission intensity on a much longer scale of ~ 100 ns.

The temporal fluctuations of the emission spectrum were measured by a spectrometer equipped with an intensified CCD camera [ICCD, see methods and Fig. S2 (*22*)]. The time-resolved emission spectrum (Fig. 3E) consists of multiple lasing peaks at any given time. Each peak persists for tens or even hundreds of nanoseconds, and is then replaced by new peaks at different wavelengths.

To quantify the time scales of the spatio-temporal and spectro-temporal dynamics, we calculated the autocorrelation functions of the spatio- and spectro-temporal data and determined the corresponding correlation times [see Fig. S4 and methods (*22*)]. The correlation times are $\tau_{\rm corr}^{(\lambda)} = 94$ ns and $\tau_{\rm corr}^{(x)} = 83$ ns, respectively, for the measurements shown in Fig. 3. Therefore, the spatio- and spectro-temporal dynamics of the D-cavity laser feature the same characteristic time scales. They are about two orders of magnitude slower than those of the stripe laser

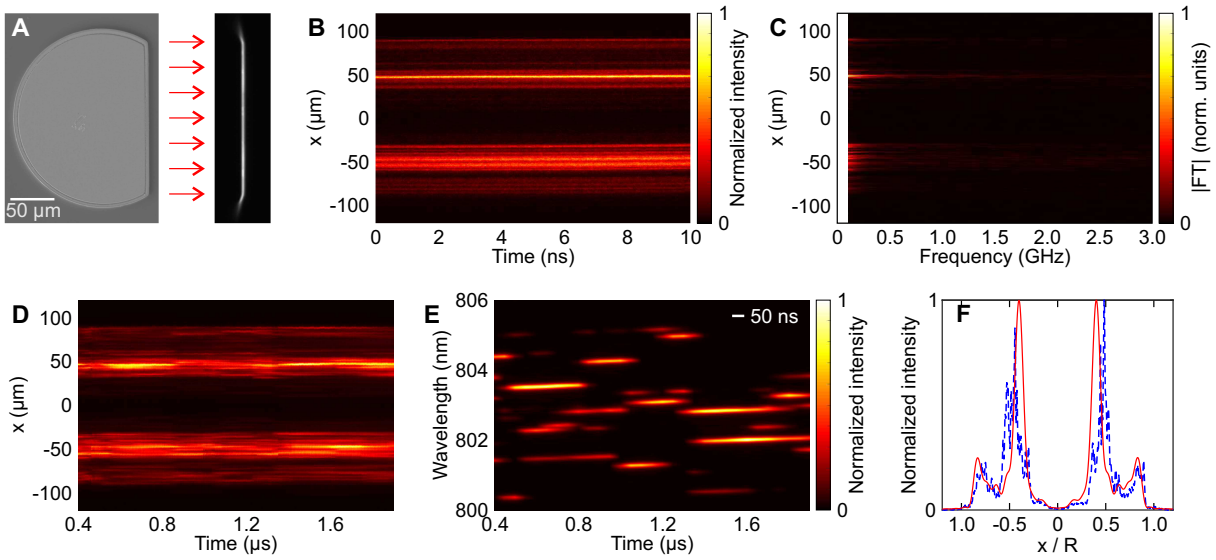

Figure 3: Lasing dynamics in a D-cavity with 100 μm radius fabricated by reactive ion etching. (**A**) Top view SEM image and optical image of the electroluminescence on the straight boundary segment. The pump current for the electroluminescence image was 3 mA, well below the lasing threshold of $I_{th} = 150$ mA. The intensity profile is homogeneous. (**B**) Spatio-temporal image of the emission intensity, $I(x,t)$, at the straight segment for 500 mA pump current during a 10 ns-long interval at 1.4 μs after the start of a 2 μs-long pump pulse. (**C**) Temporal Fourier transform of $I(x,t)$ in (B), demonstrating the absence of nanosecond-scale oscillations. (**D**) Spatio-temporal image of the emission intensity during the interval 0.4–1.9 μs. (**E**) Spectro-chronogram for the same pump conditions as in (D), measured with 50 ns temporal resolution. (**F**) Lasing emission intensity distribution at the straight segment for 500 mA pump current, measured with the CCD camera and integrated over a 2 μs-long pulse (blue dashed line), and numerically calculated emission profile of high-Q modes (red solid line).

(≤ 1 ns). These results were further confirmed by measurements of other D-cavity lasers with different size.

As seen in Figs. 3, B and D, the lasing emission from the straight segment of the D-cavity is spatially inhomogeneous. This inhomogeneity is not caused by defects on the sidewall, as confirmed by the smooth electroluminescence profile in Fig. 3A. When the pump current increases, a spatially inhomogeneous emission pattern gradually develops (see Fig. S7). The intensity profile for 500 mA, plotted as dashed blue line in Fig. 3F, exhibits two distinct length scales. The coarse scale, of the order of several tens of micrometers, represents the size of the dark region in the middle and the bright regions of strong emission around it. The fine scale, of the order of a few micrometers, is the width of the narrow peaks inside the bright regions. Experimentally, the coarse scale is proportional to the cavity size (see Fig. S7), while the fine scale is limited by the spatial resolution of the imaging optics. According to numerical simulations [see methods (*22*)], the coarse-scale emission profile reflects the sum of the intensity distributions of the passive D-cavity modes with high quality (Q) factors. Those high-Q modes within the gain spectrum correspond to the lasing modes due to their low thresholds, and their intensity distributions determine the total emission profile. The calculated emission intensity profile shown as red solid line in Fig. 3F [also see Fig. S9 (*22*)] agrees well with the coarse structure of the measured emission profile. While the coarse structure is maintained throughout the pulse, the fine-scale peaks appear or disappear over the course of the pulse as different lasing modes turn on or off.

Next we show that the remaining fluctuations of the laser emission from wave-chaotic cavities result from thermal effects. The current injection causes sample heating, which modifies the refractive index of the cavity and the gain spectrum of the quantum well. Consequently, the lasing modes may change, leading to dynamic variations of the emission spectra as well as the spatial emission intensity distributions. In order to investigate the thermal effects, we increased

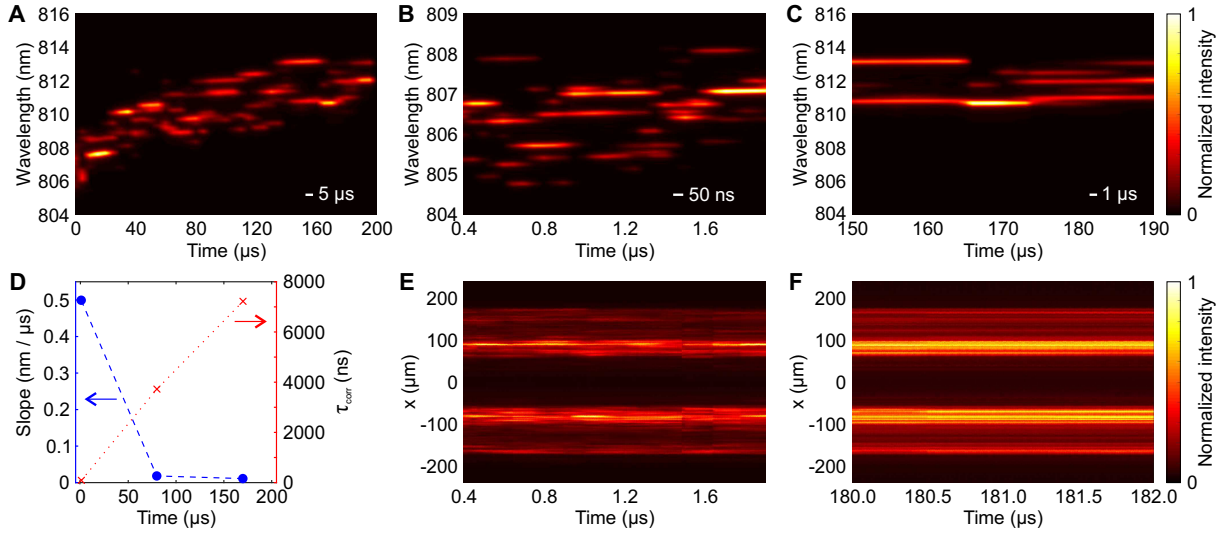

Figure 4: Thermal effect on the lasing dynamics. A D-cavity laser fabricated by reactive ion etching with $R = 200$ μm radius was pumped by a $t_p = 200$ μs pulse. The pump current was 800 mA, where the lasing threshold was $I_{th} = 300$ mA. (**A**) Spectrochronogram of the lasing emission for 0–200 μs measured with 5 μs temporal resolution. The spectral shift to longer wavelengths is caused by an increase of the sample temperature. (**B**) Spectrochronogram for 0.4–1.9 μs measured with 50 ns temporal resolution. (**C**) Spectrochronogram for 150–190 μs measured with 1 μs temporal resolution. (**D**) Rate of the red-shift of the center of mass of the emission spectra (blue circles) and the spectral correlation times $\tau_{\mathrm{corr}}^{(\lambda)}$ (red crosses) at different times during the 200 μs pulse. The red-shift slope decreases by almost two orders of magnitude as the sample temperature stabilizes, and conversely the spectral correlation time increases by two orders of magnitude. (**E**) Spatio-temporal image of the lasing emission during 0.4–1.9 μs and (**F**) during 180–182 μs, showing the spatio-temporal dynamics becomes more stable with time.

the pump pulse length t_p to 200 μs. After the turn-on of the pump current, the sample temperature first rose quickly, then gradually stabilized. If heating effects were relevant, the lasing dynamics would slow down over time.

Figure 4A presents the spectro-temporal data for a D-cavity laser with $R = 200$ μm. Over the time interval of $t_p = 200$ μs, the lasing spectrum exhibits a continuous shift to longer wavelengths due to the increase of the sample temperature. However, the red shift of the lasing spectrum notably slows down during the later part of the pump pulse, and individual peaks last longer in time. We computed the center of mass (COM) for the time-resolved spectrum $\lambda_{\rm COM}(t)$, and found it is fitted well by an exponential function $\lambda_{\rm COM}^{\rm (fit)}(t) = \lambda_0 - \lambda_1 \exp(-t/\tau_{th})$, with the decay time $\tau_{th} = 174$ μs [see methods (*22*)]. The slope $d\lambda_{\rm COM}^{\rm (fit)}(t)/dt$ gives the rate of the spectral shift. The sample temperature gradually stabilizes during the pulse as indicated by the decreasing slope of $\lambda_{\rm COM}(t)$ from 0.5 nm/μs during the first two microseconds to 0.01 nm/μs at 170 μs (see Fig. 4D).

To characterize the change of the time scale of the emission fluctuations, we measured the time-resolved spectra at different times during the 200 μs pulse with better temporal resolution. The spectral correlation time for a D-cavity laser increases from $\tau_{\rm corr}^{(\lambda)} = 90$ ns during the first 2 μs (Fig. 4B) to 7.2 μs during 150–190 μs (Fig. 4C). Figure 4D shows the correlation times and slope of $\lambda_{\rm COM}$ at different times during the pulse, illustrating how the emission fluctuations slow down as the temperature stabilizes. Spatio-temporal measurements also confirmed the lasing dynamics become more stable with time (Fig. 4, E and F).

These results illustrate the effect of the temperature change on the lasing dynamics, and indicate that better thermal management can lead to a further stabilization of the temporal dynamics of wave-chaotic lasers. This is in stark contrast to the wide stripe lasers which did not exhibit a stable dynamics at all. Fast oscillations and pulsations on a nanosecond time scale persisted until 200 μs, even though the emission spectra indicated the sample had reached a

thermal equilibrium after ~ 50 μs [Fig. S6 (*22*)].

We also tested the D-cavity lasers fabricated by wet chemical etching. Although the cavity sidewalls are not vertical and rougher than for fabrication by reactive ion etching, the spatio- and spectro-temporal dynamics of the lasing emission is very similar [Fig. S11 (*22*)]. These results demonstrate the robustness of the stable lasing dynamics in a wave-chaotic cavity against fabrication imperfections. However, the spatial emission profile differs from that of a dry-etched cavity. This is attributed to the modification of the mode structures by the rough boundary, and confirmed by numerical simulations [Fig. S12 (*22*)]. Even in the presence of boundary roughness, the complex wave interference persists in the wave-chaotic cavities and suppresses the formation of filamentation and spatio-temporal instabilities. Consequently the lasing emission profile is dictated by the passive cavity mode structure.

Lasing dynamics in disordered cavities

While the wave-chaotic cavities can efficiently suppress lasing instabilities, they lack emission directionality due to the absence of a predominant propagation direction. Therefore the question arises if we can suppress lasing instabilities via complex wave interference while having directional emission.

We consider a simple 1D dielectric slab cavity with random fluctuations of the refractive index (Fig. 5B). The index fluctuations generate multiple reflected waves that interfere subsequently. Thus, the resonant modes no longer have a constant frequency spacing and their spatial profiles become irregular with varying spatial scales (Figs. 5B and S13), reminiscent of the modes in a 2D wave-chaotic cavity (Fig. S8).

To simulate their lasing dynamics, we solved the semiconductor Maxwell-Bloch equations in the time domain. Our full-wave model goes beyond the slowly varying envelope / rotating wave (in time) and paraxial (in space) approximations, fully resolving the spatio-temporal dy-

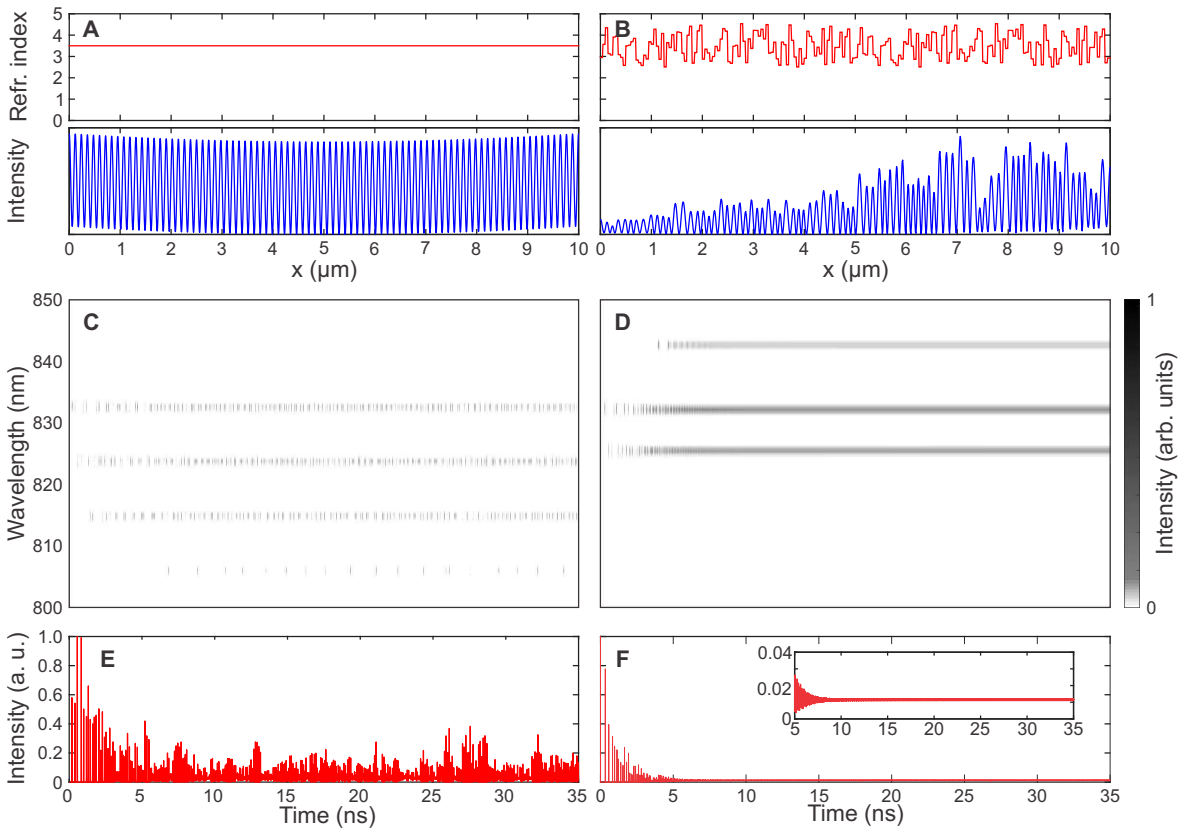

Figure 5: Simulation of the lasing dynamics in one-dimensional cavities with homogeneous refractive index profile and spatially-varying index profile, respectively, at the same pump current density $J = 500$ A cm^{-2}. (**A, B**) Spatial distribution of the refractive index (red line) and the field intensity (blue line) for a mode at $\lambda = 833.3$ nm in the homogeneous cavity (A) and for a mode at $\lambda = 833.8$ nm in the disordered cavity (B). (**C, D**) Spectrochronogram of the emission intensity from the homogeneous cavity (C) and from the disordered cavity (D). (**E, F**) Total output intensity for the homogeneous cavity (E) and for the disordered cavity (F).

namics on sub-optical cycle and sub-wavelength scales [see methods (*22*)]. The population inversion-dependent optical gain has an asymmetric spectrum, which closely reproduces that of a semiconductor quantum well. Taking into account the dynamical coupling between the light field and the carrier system, we include all spatio-temporal and nonlinear effects such as spatial hole burning and multiple wave mixing mediated by the carriers (*29,30*).

We compare the simulated lasing dynamics of a disordered cavity to that of a homogeneous cavity with regular mode structure in Fig. 5A. The disordered cavity features stable lasing dynamics over a wide range of pump currents, while lasing in the homogeneous cavity is stable only just above threshold and becomes unstable with increasing pump current [Figs. S14 and S15 (*22*)]. For example, when the pump current is about five times of the threshold ($J_{th} = 104$ A cm^{-2}), four longitudinal modes lase in the homogeneous cavity, and all modes pulsate irregularly on a sub-nanosecond time scale (Fig. 5C). The total emission intensity in Fig. 5E fluctuates in time, and does not approach a constant value even well beyond the transient dynamics. These instabilities are caused by the nonlinear interactions between the lasing modes and the gain medium through processes such as spatial hole burning and multi-wave-mixing (*31*).

The disordered cavity with almost identical lasing threshold ($J_{th} = 96$ A cm^{-2}) as the homogeneous cavity has three modes lasing at the same pump current density. After some initial pulsations, each lasing mode reaches a steady state (Fig. 5D). The total output intensity also approaches a constant value beyond the transient period (Fig. 5F). The stable state of multimode lasing sets in faster at higher pump current [Fig. S15 (*22*)].

Therefore, even in a 1D cavity, the interference of multiple scattered waves with random phases can lead to stable lasing dynamics, and the stabilization is complete in the absence of thermal effects. These results confirm the generic nature of our scheme to suppress spatio-temporal instabilities by increasing the spatial complexity of the lasing modes.

Discussion and conclusion

Our approach for obtaining a stable state of multimode lasing in broad-area edge-emitting semiconductor lasers is fundamentally different from previous ones in several respects. Most previous approaches aim at suppressing the spatio-temporal instabilities and the formation of self-organized structures like filaments by minimizing the number of lasing modes. Our approach maintains multimode lasing while achieving stable temporal dynamics by tailoring the spatial properties of the lasing modes using resonators with chaotic ray dynamics or with random refractive index fluctuations. Although the mechanisms causing lasing instabilities in 1D and 2D cavities are different, both are disrupted by complex wave interference. Since this process is present across the whole cavity, we attain global suppression of the instabilities, in contrast to schemes like injection and feedback that can influence the dynamics only locally.

It is important to note that our scheme of achieving stable multimode operation is very robust with respect to perturbations such as boundary roughness, since they do not qualitatively change the already pseudo-random structure of the lasing modes. Although small modifications of the cavity geometry of broad-area edge-emitting semiconductor lasers were considered previously (*32*–*35*), a dominant propagation direction and thus well-defined wave fronts were maintained, and the spatial scales of the modes were not significantly modified, in stark contrast to the wave-chaotic and disordered cavities presented here.

Although the multimode operation of D-cavity lasers produces emission with relatively low spatial coherence (*36*), which prevents tight focusing, the temporal stability of the lasing power and the emission profile, as shown in this work, is essential to produce stable beam profiles necessary for many high-power applications. For example, laser processing of materials and devices requires diverse beam shapes such as circular flat-top, square, rectangle or line profiles, and various beam-shaping techniques have been developed in recent years (*37*). Low spatial

coherence of the laser beams prevents coherent artifacts and enables smooth intensity profiles, e.g., the D-cavity laser emission may be coupled to a multimode fiber to produce a stable flat-top beam free of speckle. Another potential application is pumping high-power multimode fiber lasers and amplifiers.

In previous studies, broad-area VCSELs with pulsed pumping demonstrated non-modal emission with low spatial coherence, when the interplay between a rapid thermal chirp and the build-up of a thermal lens breaks up the global cavity modes (*38*). As the VCSEL becomes thermally stable with time, the multimode operation resumes and fast temporal dynamics appears. This is fundamentally different from the wave-chaotic cavities in which the stable state of lasing is maintained in multimode operation. It should be mentioned that random fiber lasers can also exhibit temporal fluctuations (*39*), which disappear for stronger pumping. Both the mechanism inducing the instabilities (interplay between stimulated Brillouin scattering (SBS) and Rayleigh scattering) and that quenching the instabilities (suppression of SBS) are distinct from those for the 1D disordered semiconductor lasers we simulated [see supplementary materials (*22*)].

We therefore propose the demonstrated suppression of lasing instabilities by means of complex multi-wave interference as a new paradigm for manipulating the temporal dynamics of multimode lasers. We believe it is generally applicable to other high-power lasers exhibiting instabilities such as broad-area VCSELs and solid-state lasers, as well as multimode fiber lasers and amplifiers. By deforming the cavity or fiber cross section or introducing random refractive index fluctuations, the spatial mode structure becomes speckled, preventing lens formation and self-focusing instabilities. On a more general level, this work opens a new direction of research combining concepts from both wave-dynamical chaos and deterministic chaos. This combination and its implications have been barely investigated so far in lasers or other nonlinear wave-dynamical systems. We expect the idea of manipulating nonlinear temporal dynamics by disrupting the formation of self-organized structures will have a significant impact not only on

laser physics but will find applications in other systems with complex spatio-temporal dynamics as well.

References

1. M. P. Hassell, H. N. Comins, R. M. Mayt, *Nature* **353**, 255 (1991).
2. I. R. Epstein, K. Showalter, *J. Phys. Chem.* **100**, 13132 (1996).
3. J. P. Graves, *et al.*, *Nature Comm.* **3**, 624 (2012).
4. E. Altshuler, T. H. Johansen, *Rev. Mod. Phys.* **76**, 471 (2004).
5. N. B. Abraham, L. A. Lugiato, L. M. Narducci, *J. Opt. Soc. Am. B* **2**, 7 (1985).
6. G. Huyet, M. C. Martinoni, J. R. Tredicce, S. Rica, *Phys. Rev. Lett.* **75**, 4027 (1995).
7. J. Othsubo, *Semiconductor Lasers - Stability, Instability and Chaos* (Springer, Heidelberg, 2013).
8. I. Fischer, O. Hess, W. Elsäßer, E. Göbel, *Europhys. Lett.* **35**, 579 (1996).
9. O. Hess, *Chaos, Solitons & Fractals* **4**, 1597 (1994).
10. O. Hess, T. Kuhn, *Phys. Rev. A* **54**, 3360 (1996).
11. J. Marciante, G. Agrawal, *IEEE J. Quantum Electron.* **33**, 1174 (1997).
12. J. R. Marciante, G. P. Agrawal, *IEEE Photon. Technol. Lett.* **10**, 54 (1998).
13. D. Scholz, *et al.*, *Opt. Express* **16**, 6846 (2008).
14. M. Arahata, A. Uchida, *IEEE J. Sel. Top. Quant. Electron.* **21**, 1800609 (2015).

15. T. Pawletko, M. Houssin, M. Knoop, M. Vedel, F. Vedel, *Opt. Comm.* **174**, 223 (2000).

16. S. Takimoto, T. Tachikawa, J. Ohtsubo, *IEEE Phot. Tech. Lett.* **21**, 1051 (2009).

17. J. Martín-Regalado, G. H. M. van Tartwijk, S. Balle, M. S. Miguel, *Phys. Rev. A* **54**, 5386 (1996).

18. S. K. Mandre, I. Fischer, W. Elsäßer, *Opt. Comm.* **244**, 355 (2005).

19. C. Zink, M. Niebuhr, A. Jechow, A. Heuer, R. Menzel, *Opt. Express* **22**, 14108 (2014).

20. H. Hodaei, M.-A. Miri, M. Heinrich, D. N. Christodoulides, M. Khajavikhan, *Science* **346**, 975 (2014).

21. W. Liu, *et al.*, *Nature Comm.* **8**, 15389 (2017).

22. Materials and methods are available as supplementary materials.

23. H. E. Türeci, H. G. L. Schwefel, P. Jacquod, A. D. Stone, *Progress in Optics* **47**, 75 (2005).

24. T. Harayama, S. Shinohara, *Laser & Photonics Review* **5**, 247 (2010).

25. H. Cao, J. Wiersig, *Rev. Mod. Phys.* **87**, 61 (2015).

26. H.-J. Stöckmann, *Quantum Chaos: An Introduction* (Cambridge University Press, Cambridge, 2000).

27. Y.-F. Xiao, *et al.*, *Frontiers Optoelectron. China* **3**, 109 (2010).

28. X. Jiang, *et al.*, *Science* **358**, 344 (2017).

29. S. Guazzotti, A. Pusch, D. E. Reiter, O. Hess, *Phys. Rev. B* **94**, 115303 (2016).

30. K. Böhringer, O. Hess, *Prog. Quant. Electron.* **32**, 159 (2008). *ibid* **32**, 247 (2008).

31. L. Furfaro, *et al.*, *IEEE J. Quantum Electron.* **40**, 1365 (2004).

32. H. Adachihara, O. Hess, E. Abraham, P. Ru, J. V. Moloney, *J. Opt. Soc. Am. B* **10**, 658 (1993).

33. G. Levy, A. Hardy, *IEEE J. Quantum Electron.* **33**, 26 (1997).

34. C. Simmendinger, D. Preiber, O. Hess, *Opt. Express* **5**, 48 (1999).

35. A. Büttner, U. D. Zeitner, R. Kowarschik, *J. Opt. Soc. Am. B* **22**, 796 (2005).

36. B. Redding, *et al.*, *Proc. Nat. Acad. Sci.* **112**, 1304 (2015).

37. K. Fuse, *Laser Technik Journal* **12**, 19 (2015).

38. S. K. Mandre, W. Elsäßer, I. Fischer, M. Peeters, G. Verschaffelt, *Opt. Express* **16**, 4452 (2008).

39. S. K. Turitsyn, *et al.*, *Nature Photonics* **4**, 231 (2010).

40. R. Buschlinger, M. Lorke, U. Peschel, *Phys. Rev. B* **91**, 045203 (2015).

41. S. Sunada, T. Harayama, K. S. Ikeda, *Phys. Rev. E* **71**, 046209 (2005).

42. J. Andreasen, P. Sebbah, C. Vanneste, *Phys. Rev. A* **84**, 023826 (2011).

Acknowledgments

H.C. and S.B. thank A. Douglas Stone, Hakan Tureci, Li Ge, Jonathan Andreasen and Christian Vanneste for fruitful discussions.

Funding. The work conducted at Yale University is supported partly by the Office of Naval Research (ONR) with a MURI grant N00014-13-1-0649, and by the Air Force Office of

Scientific Research (AFOSR) under grant no. FA9550-16-1-0416. The research at Imperial College London is partly supported by the Engineering and Physical Sciences Research Council (EPSRC) UK through the projects EP/L024926/1 and EP/L027151/1, by the AFOSR under grant no. FA9550-14-1-0181, and with funding by the European Regional Development Fund through the Welsh Government. For the work at Nanyang Technological University, funding support is acknowledged from the Singapore Ministry of Education Tier 2 Program (MOE 2016-T2-1-128) and the Singapore National Research Foundation Competitive Research Program (NRF-CRP18-2017-02).

Author contributions. S.B. conducted experimental characterization and data analysis, and prepared the manuscript. H.Y., Y.Z., X.H. and Q.W. did sample fabrications. K.K. calculated the resonant modes in D-cavities. S.G. and S.S.O. modeled the semiconductor laser dynamics. O.H. guided the theory of complex semiconductor laser dynamics and edited the paper. H.C. proposed the idea, initiated the research and edited the paper.

Competing interests. The authors declare no competing financial interests.

Data and materials availability. All data needed to evaluate the conclusions in the paper are present in the paper or the supplementary materials.

Supplementary Materials

Materials and Methods

Supplementary Text

Table S1

Fig S1 - S15

References (*40–42*)